MDPI

Article

Spatiotemporal Changes in Extreme Precipitation in China's Pearl River Basin during 1951–2015

Shirong Cai [1], Kunlong Niu [1], Xiaolin Mu [1], Xiankun Yang [1,2,*] and Francesco Pirotti [3,4]

1   School of Geography and Remote Sensing, Guangzhou University, Guangzhou 510006, China;
    caisr@e.gzhu.edu.cn (S.C.); 2112101068@e.gzhu.edu.cn (K.N.); 2112101067@e.gzhu.edu.cn (X.M.)
2   Rural Non-Point Source Pollution Comprehensive Management Technology Center of Guangdong Province,
    Guangzhou University, Guangzhou 510006, China
3   Department of Land, Environment, Agriculture and Forestry (TESAF), University of Padova,
    Viale dell'Università 16, 35020 Legnaro, Italy; francesco.pirotti@unipd.it
4   Interdepartmental Research Center of Geomatics (CIRGEO), University of Padova, Viale dell'Università 16,
    35020 Legnaro, Italy
*   Correspondence: yangxk@gzhu.edu.cn

Abstract: Precipitation is a key component of the hydrological cycle and one of the important indicators of climate change. Due to climate change, extreme precipitation events have globally and regionally increased in frequency and intensity, leading to a higher probability of natural disasters. This study, using the long-term APHRODITE dataset, employed six precipitation indices to analyze the spatiotemporal changes in extreme precipitation in the Pearl River Basin during 1951–2015. The Mann–Kendall (M–K) test was used to verify the significance of the observed trends. The results indicate that: (1) the interannual PRCPTOT showed a trend with an average positive increase of 0.019 mm/yr, which was followed by an increase in SDII, R95P, and RX1day, and a decrease in R95D and CWD; seasonal PRCPTOT also displayed an increase in summer and winter and a decrease in spring and autumn, corresponding to increases in R95P and SDII in all seasons. (2) The annual precipitation increases from the west to east of the basin, similar to the gradient distribution of SDII, R95P and RX1day, with the high R95D happening in the middle and lower reaches of the Xijiang River, but the CWD increased from the north to south of the basin. The seasonal spatial distributions of PRCPTOT, SDII, and R95P are relatively similar except in autumn, showing an increase from the west to east of the basin in spring and winter and a gradual increase from the north to south of the basin in summer, indicating that the Beijiang and Dongjiang tributary basins are more vulnerable to floods. (3) The MK test results exhibited that the Yunnan–Guizhou Plateau region in the upper reaches of the Xijiang River Basin became drier, and there was an increase in extreme precipitation in the Beijiang and Dongjiang river basins. The study results facilitate valuable flood mitigation, natural hazard control and water resources management in the Pearl River Basin.

Keywords: Pearl River Basin; extreme precipitation; APHRODITE; Mann–Kendall

1. Introduction

Global warming is intensifying the global hydrological cycle [1]. Precipitation is a crucial factor in the hydrological cycle [2], and variations in precipitation (including changes in precipitation intensity, quantity, duration, and spatial distribution) may trigger extreme weather events, such as heavy rains, floods, and droughts, which will cause huge losses of life and property [3,4]. China is one of the countries experiencing more freak weather events than ever before [5]. Recent studies have revealed that there has been a decrease in the number of days with precipitation in China, but the intensity of precipitation increased dramatically [6–8]. Extreme changes in precipitation may lead to more disasters, making disaster prevention and control more difficult in China.

Precipitation can regulate the ecosystems that a population depends on, and it has far-reaching effects on socioeconomical sustainability and the security of increasingly scarce water resources [9]. Many previous studies on precipitation patterns [10–13] have shown that precipitation fluctuates across regions, and they have proved the importance of precipitation spatiotemporal patterns in the prediction of future climate change [14]. Therefore, understanding precipitation change in different regions is crucial for the identification of regional changes in climate and the mitigation of the resultant impacts.

Numerous studies have investigated the changes of precipitation in China. Zhai et al. [15] showed that the overall precipitation in China did not change much from 1951 to 2000, but there were significant annual and seasonal variations in some regions; Zhang et al. revealed that during 1956–2000, there has been a decrease in spring and autumn precipitation, corresponding to an increasing in winter in China [16]. The results from Song et al. [17] showed that the spatiotemporal changes of precipitation in different regions varied greatly from 1961 to 2008.

Some studies also conducted such investigations at the scale of large river basins as an integrated hydrological cycle [18]. Understanding the changes in precipitation at this scale is a prerequisite for sustainable water resource management in large river basins [19]. Jiang et al. [20] observed increased precipitation during monsoon season in the Yangtze River Basin from 1961 to 2000, especially in June and July. Zhang et al. [21] reported a possible increase in droughts caused by reduced spring and autumn precipitation, but they also stated an increase in winter precipitation in the Yellow River Basin during 1960–2009. In the Pearl River Basin (PRB), Liu et al. [22] believed that the changes in annual and seasonal precipitation are not statistically significant from 1959 to 2009. These studies were often executed based on the observations from meteorological stations, but the results for the remote and rural areas were derived with high uncertainty due to the sparsity of stations in the remote and rural regions [23–25]. Thus, there are still significant discrepancies in the uncertainty on precipitation change assessment in different regions of different large river basins.

The Pearl River ranks as the third largest river in China. The uneven spatiotemporal distribution of precipitation in the PRB has been becoming a serious obstacle for the efficient utilization of water resources and effective flood mitigation [3,26]. Since China implemented the reform and opening-up policy in the 1970s, the PRB, especially in the delta region, has made meaningful contributions to China's socioeconomic development. However, basin-wide and local floods have been intensified by climate change and enhanced socioeconomic activities [27]. The resultant extreme water events have further caused a degradation in the water quality and river ecosystem in the PRB [28]. Previous studies primarily concentrated on extreme precipitation and resultant flood risks in the PRB. Yang et al. [29] revealed that there were differences in the seasonal extreme precipitation in varied regions based on frequency analysis to explore the spatiotemporal pattern of changes in precipitation in the PRB. Duan et al. [30] used peak-over-threshold sampling, a modified Mann–Kendall (M–K) test and Poisson regression to study precipitation changes, and the results showed that seasonal changes in extreme precipitation more easily cause floods, droughts and regional warming in the PRB. Zhang et al. [31] utilized precipitation indices to explore the spatiotemporal changes of precipitation, and they found that the decrease in precipitation happened primarily in the upper and middle reaches of the Pearl River, while the extreme precipitation could further increase in the lower reaches in the future. These studies investigated the average precipitation and extreme precipitation events, providing valuable information for identifying the characteristics of spatiotemporal variation of precipitation.

Most of the aforementioned studies are based on precipitation records acquired before 2005. There are few studies revealing the changes of extreme precipitation in the PRB derived from the precipitation data obtained in the last 20 years. Therefore, the latest trends of extreme precipitation changes in the PRB remained unclear. In light of the complex process of extreme precipitation change in different regions, assessing its spatiotemporal

pattern is still a challenging task. Regarding recent climate change and intensified human activities due to fast urbanization, the spatiotemporal changes of precipitation are becoming more complex and uncertain in the PRB. It is necessary to carry out further study to analyze precipitation pattern changes. To evaluate and test trends of extreme precipitation changes in the PRB, this study, based on the APHRODITE dataset, employed six precipitation indices. We analyzed the spatial and temporal characteristics of extreme precipitation from 1951 to 2015, and we used the M–K test to identify notable trends. We also discuss the spatiotemporal variability of these indices in order to provide a reference for disaster prevention and water resource management in the PRB.

2. Materials and Methods

2.1. Study Area

The PRB is situated in southern China, from $102°14'$ E to $115°53'$ E and $21°31'$ N to $26°49'$ N, with a basin size of 4.4×10^5 km^2. The PRB is a composite water system with 3 major tributaries [32]: the Xijiang River, Beijiang River, and Dongjiang River (Figure 1). The Xijiang River is the largest, accounting for 77.8% (3.5×10^5 km^2) of the overall PRB; the Beijiang River is the second largest, with a size of 4.6×10^4 km^2; the Dongjiang River covers an approximate area of 2.7×10^4 km^2, accounting for only 6.6% of the overall PRB. The water quality and natural environment of Dongjiang River are the best among the three tributaries, and approximately 80% of Hong Kong's water supply is sourced from the Dongjiang River [33].
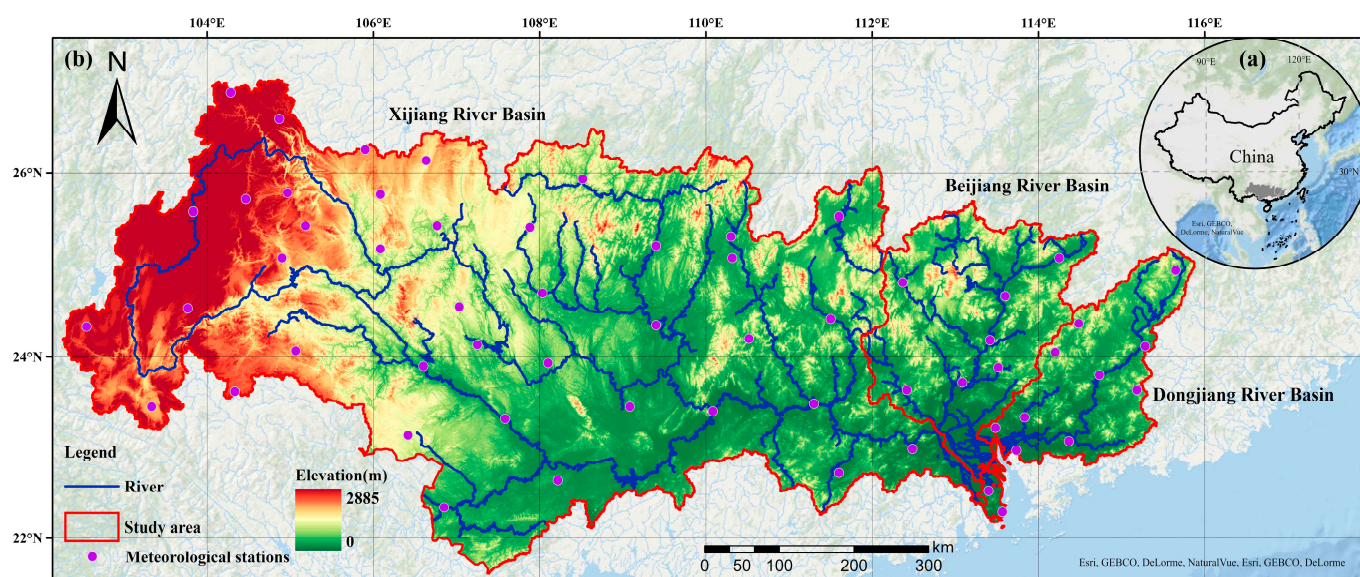
Figure 1. (**a**) Rough location of the PRB in China; (**b**) topographical characteristics and the distribution of meteorological stations in the PRB.

The PRB is located in the tropical and subtropical climates, where the annual average temperature ranges from 14 to 22 °C, the annual average precipitation is between 1200 and 2000 mm, and the annual average runoff measures 338.1 billion m^3 [34]. In the PRB, the elevation decreases from west to east, with mountains and karst geomorphology mainly in the northwest and hills and plains in the southeast of the basin [35].

Influenced by the subtropical monsoon, the precipitation varies greatly in seasonal and interannual distribution: about 70% to 85% of the precipitation happens in the monsoon season (April to September); precipitation in the wet years can reach as high as 6 to 7 times that in the dry years, which makes the area prone to the occurrence of natural hazards [36]. Typhoons and rainstorms in the PRB are characterized by high intensity, high frequency, and long duration in April to October, which is the main reason for floods. In recent years, the annual patterns of runoff in the Pearl River has become more uneven and floods happened more frequently in the monsoon season [37]. The droughts of the PRB are also

controlled by precipitation, especially the mid- and long-term droughts, which are mainly regulated by seasonal precipitation changes [38].

Since the 1980s, the PRB has undergone rapid economic development. However, the economic development is unevenly distributed: the upper reaches (Yunnan, Guizhou, and Guangxi provinces) are in the wild environments with slow economic development, while the Pearl River Delta (PRD) is a very prosperous region. With the fast industrialization and urbanization in the PRD, the impact of extreme precipitation on the socioeconomic losses is more dramatic. Uncertain precipitation changes have directly impaired water resources management and flood prevention in the PRB.

2.2. Data

2.2.1. APHRODITE Data

Previous studies mainly used the data from meteorological stations to characterize precipitation changes, but owing to the uneven distribution of meteorological stations, the results obtained in remote areas with sparse stations were obtained with high uncertainty [23–25]. The reanalysis datasets from ground observations and satellite monitoring can provide better spatiotemporal coverage for precipitation analysis [39–42], such as TRMM (The Tropical Rainfall Measuring Mission), GPCP (Global Precipitation Climatology Project), etc. Those products were mostly established at the global scale but with low spatial resolution unsustainable for evaluating regional precipitation changes. The APHRODITE (Asian Precipitation Highly Resolved Observative Data Integration Towards Evaluation) dataset provides high-quality daily precipitation products for Asian subregions. Compared to other reanalysis datasets, it has a better spatial resolution of $0.25° \times 0.25°$, which can derive the spatiotemporal patterns and climate characteristics in a relatively small region. It also performed well in the Tibetan Plateau and South Asia [43–45]. Therefore, it is often used to verify precipitation analysis in Asia [46,47].

APHRODITE's gridded precipitation dataset is the only continental-scale daily product that covers a long term from 1951 onwards, and it features an extensive collection of daily rainfall obtained from rain gauges stationed in Asia (http://aphrodite.st.hirosaki-u.ac.jp, accessed on 13 May 2022). The interpolation algorithm incorporates the orographic correction of precipitation and an improved quality-control method. The APHRODITE dataset can better represent the real precipitation situation. The gridding procedure and accuracy of APHRODITE data were thoroughly discussed by Hamada et al. [48] and Yatagai et al. [49,50].

In this study, we use APHRO_MA_025deg_V1101 (1951–2007) and APHRO_MA_025deg_V1101EX_R1 (2008–2015) datasets. Both products were produced by the same algorithm, which is compatible and comparable with each other. The 1951–2015 daily precipitation data across the whole PRB were obtained with a spatial resolution of $0.25°$. According to the physical conditions of the PRB, we considered a daily value of less than 1 mm as a non-rainfall day and used python-based programming to generate seasonal and annual values.

2.2.2. Meteorological Station Data

We also collected daily data of 59 meteorological stations in the PRB from 1951 to 2015. The precipitation data were derived from China's surface climate daily dataset V3.0 managed by the China Meteorological Administration (http://data.cma.cn, accessed on 9 June 2022). The dataset has undergone strict quality control [51] and is one of the most reliable daily precipitation datasets in China.

The dataset contains a few missing values, accounting for less than 0.01% of the overall dataset. The missing values were processed as follows: the missing values for a station were filled by the data of adjacent stations with simple linear regression interpolation; if there are more than 30 consecutive days of missing values in a station, this time series will be excluded from further analysis. In fact, this filling operation has no significant influence on data validation. The daily data were then integrated into annual precipitation

data and interpolated by the Kriging method to evaluate the accuracy of APHRODITE precipitation data.

2.2.3. Other Reanalysis Datasets

To show the accuracy of AHPRODITE datasets, we also employed two new datasets for comparison.

MSWEP (Multi-Source Weighted-Ensemble Precipitation) is a global precipitation dataset that integrates information from multiple data sources, including satellite observations, ground-based measurements, and reanalysis models [52]. The dataset has a spatial resolution of 0.1° and covers the period from 1979 to near real time.

CHIRPS (Climate Hazards Group InfraRed Precipitation with Station data) is a high-resolution, long-term daily precipitation dataset [53]. It was developed by the Climate Hazards Group at the University of California, Santa Barbara, using satellite imagery and ground-based observations. The data cover the entire globe, from 50° N to 50° S, with a spatial resolution of approximately 0.05°. The dataset spans from 1981 to the present and is updated in near real time.

2.3. Methods

2.3.1. Precipitation Indices

We utilized six extreme precipitation indices (EPIs) suggested by the Joint CCl/CLIVAR/ JCOMM ETCCDI (http://etccdi.pacificclimate.org, accessed on 15 December 2022) to explore temporal and spatial precipitation distributions in the PRB (Table 1). These EPIs are widely employed to examine the variability of extreme precipitation [54–58] and demonstrate extreme precipitation trends over time.

Table 1. Descriptions of the EPIs.

Index	Indicator Name	Definition	Units
PRCPTOT	Wet day precipitation	Total precipitation from days ≥1 mm in the period	mm
SDII	Simple daily intensity index	Mean precipitation amount on wet days in the period	mm/d
R95D	Number of very wet days	The number of days when precipitation exceeds the 95th percentile of daily precipitation in the period	d
R95P	Very wet day precipitation	The sum of precipitation on days when precipitation exceeds the 95th percentile of daily precipitation in the period	mm
RX1 day	Max 1-day precipitation	Maximum 1-day precipitation of wet days in the period	mm
CWD	Consecutive wet days	Maximum number of consecutive wet days in the period	d

After arranging the sequence of precipitation values at the pixel scale, we removed the values of non-precipitation days and then calculated PRCPTOT, SDII, R95P, R95D, RX1 day, and CWD. Descriptions of the EPIs are synopsized in Table 1.

2.3.2. Mann–Kendall Trend Test

Numerous statistical approaches can be employed to detect trends in extended time series, such as moving average (MA), linear regression (LR), Mann–Kendall test (M–K), etc. The M–K test is capable of analyzing non-normally distributed data, and it is less sensitive to the presence of outliers or extreme values within the series [59], so it is commonly applied in the trend analysis for climatic and hydrological time series [60,61]. In this study, the M–K test was employed to explore the mutable trend of precipitation in the PRB. For a stable independent time series of x_t ($t = 1, 2 \ldots , n$), the indicator function S is defined as follows:

$$S = \sum_{j=1}^{n-1} \sum_{i=j+1}^{n} sgn(x_i - x_j) \tag{1}$$

where $sgn(x_i - x_j)$ is computed as follows:

$$sgn(x_i - x_j) = \begin{cases} -1 & (x_i - x_j) < 0 \\ 0 & (x_i - x_j) = 0 \\ 1 & (x_i - x_j) > 0 \end{cases} \qquad (2)$$

When $n \geq 10$, the indicator S approximately follows the Gaussian distribution. The calculation of variance $Var(S)$ is as follows:

$$Var(S) = \frac{n(n-1)(2n+5)}{18} \qquad (3)$$

where the standard normal statistical variable Z and the confidence level p are calculated as follows:

$$Z = \begin{cases} \frac{S-1}{\sqrt{Var(S)}} & S < 0 \\ 0 & S = 0 \\ \frac{S+1}{\sqrt{Var(S)}} & S > 0 \end{cases} \qquad (4)$$

$$p = 2(1 - cdf(|Z|)) \qquad (5)$$

where Z is greater than 0 represents an increasing trend and vice versa. If $|Z| \geq 1.28$, 1.64, and 2.32, these indicate that it passes the significant confidence levels of 90%, 95%, and 99%, respectively. In general, in light of the large range of spatial and temporal precipitation distribution, its statistical significance is usually lower than other climatic elements [62]. Therefore, we used the 90% confidence level in the M–K test to assess the significance of precipitation variability.

2.3.3. Sen's Slope Method

Sen's slope is a non-parametric statistical method based on median estimation [63]. It is usually applied in trend analysis of long-time series [64] and to estimate the intensity of the trend combined with the M–K test. The calculation formula is as follows:

$$\beta = median\left(\frac{x_j - x_i}{j - i}\right), j > i \qquad (6)$$

where x_i and x_j are time series data; when β is greater than 0, it indicates that the data follow an increasing trend; otherwise, it indicates a decreasing trend.

3. Results

3.1. Temporal Trends

To investigate the temporal variation of extreme precipitation in the PRB, this study calculated the temporal trends of precipitation indices based on the APHRODITE dataset. We mainly study five time series: spring (March to May), summer (June to August), autumn (September to November), winter (December, January, and February), and annual.

3.1.1. Annual Trends

As shown in Figure 2a, the annual PRCPTOT showed a slightly non-significant increase during the period 1951 to 2015, with an annual rate of 0.019 mm/yr, indicating that the PRB has been becoming wetter. The maximum, minimum, and mean annual PRCPTOT values were 1576.247 mm in 2015, 974.356 mm in 1963, and 1297.665 mm, respectively; there are 32 years that have exceeded the long-term average value, mostly occurring after 1978. The annual number of wet days (PD) showed a decreasing trend (Figure 2b), with an annual decreasing trend of −0.15 d/yr. The annual average SDII is 8.407 mm/d, with the maximum value occurring in 2008, which was 10.324 mm/d and the minimum value occurring in 1963, which was 6.647 mm/d. SDII has significantly increased ($p < 0.05$), with an annual increasing trend of 0.008 mm/d. The observed decrease in the number of wet

days and increase in daily precipitation are consistent with the results documented by Su et al. [6]. Zhang et al. [31] stated that the annual average precipitation in the PRB decreased by 2 mm/decade from 1960 to 2005, which was close to our results (1.8 mm/decade). Our results revealed an increase with a rate of 17.7 mm/yr during 2006–2015, indicating that the PRB also became humid in the past 10 years. In addition, the annual wet days' changes from Zhang et al. [31] decreased by 1.4 d/decade, and there was an increase of 0.14 mm/d per decade in annual precipitation intensity. Both results are consistent with ours.
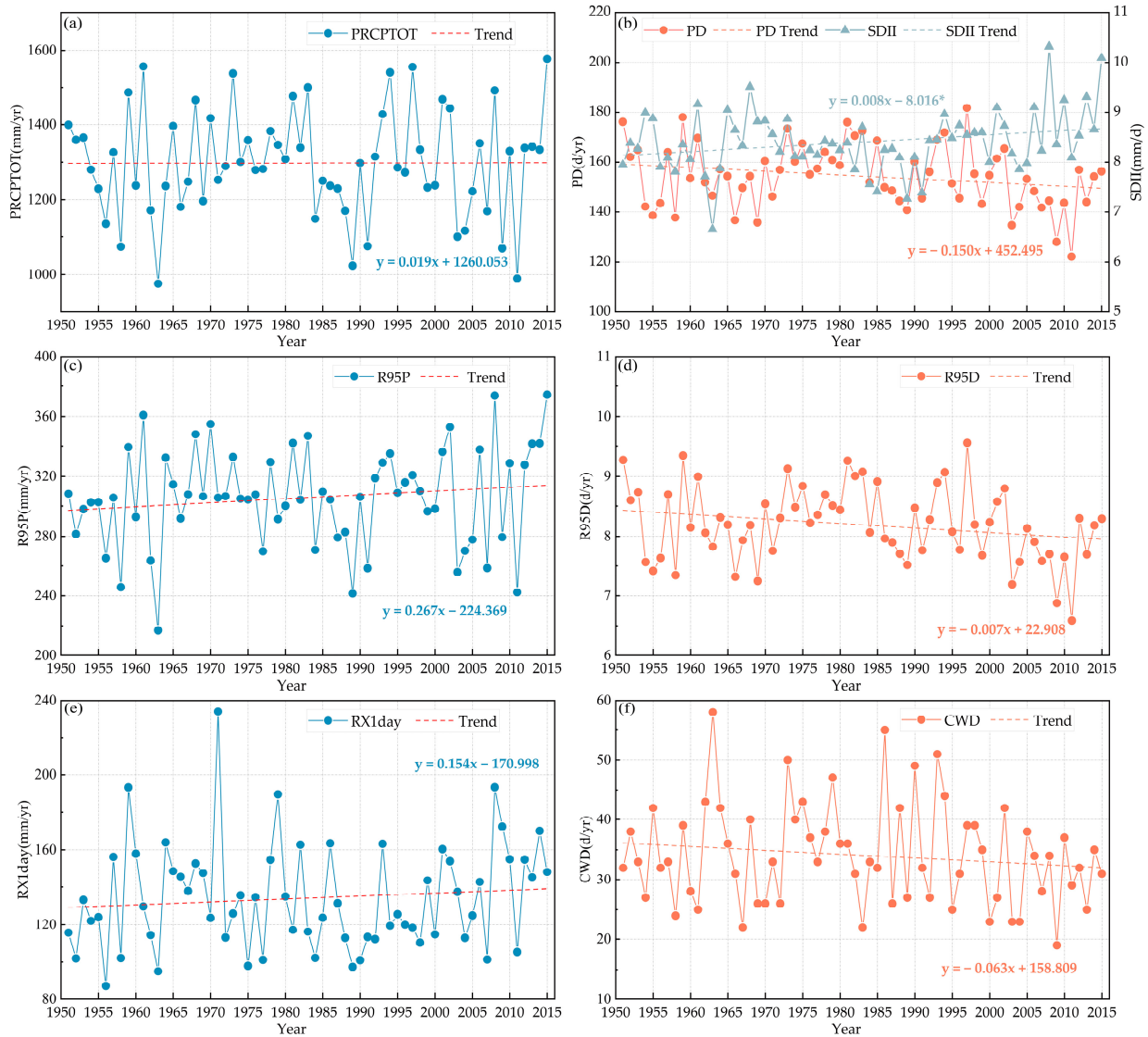
Figure 2. Temporal trends of EPIs from 1951 to 2015; (**a**) PRCPTOT, (**b**) PD and SDII, (**c**) R95P; (**d**) R95D, (**e**) RX1day, (**f**) CWD. * Significant at the level of 0.05.

During the study period, R95P showed a non-significant increasing trend (Figure 2c) with a statistically insignificant trend of 0.267 mm/yr. The maximum and minimum R95P were 32.784 mm in 2015 and 19.862 mm in 1963, respectively. We also calculated the contribution of R95P to the annual precipitation (Figure 3). The results found that the mean relative contribution of R95P was 23.59% (ranging from 20.64% to 26.88%), and the contribution showed an increasing trend of about 0.2%/decade ($p < 0.05$). The R95P result from Zhao et al. [65] increased at a rate of 0.53 mm/yr with an average contribution to annual precipitation of 28% (range from 20% to 36%), with a rate of 0.5%/decade. Our results are slightly lower than those of Zhao et al., but the trend is close.
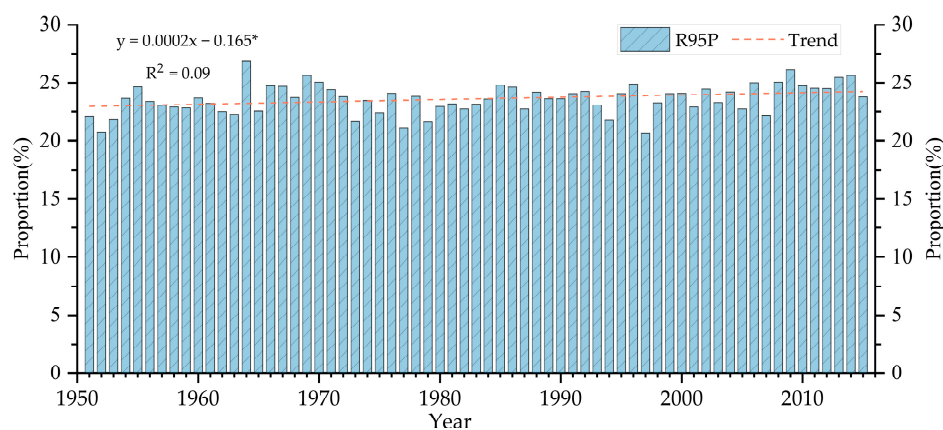
Figure 3. The relative contribution of R95P to the annual precipitation. * Significant at the level of 0.05.

The temporal trend of R95D (Figure 2d) is opposite to R95P, showing a reduction rate of −0.007 d/yr. The highest R95D appeared in 1997, which was 9.55 d; the lowest value appeared in 2011, which was 6.58 d. The findings suggest that the daily extreme precipitation has increased.

The multi-year average RX1day is 134.112 mm. The maximum value (233.929 mm) occurred in 1971; the minimum value occurred (86.948 mm) in 1956. RX1day performed an increasing trend, with a rate of 0.154 mm/yr, suggesting that the risk of short-term flooding has gradually increased. The maximum, minimum, and mean annual CWD was 58 d in 1963, 19 d in 2009, and 34.1 d, respectively. The annual CWD presented a decreasing trend, showing a rate of −0.063 d/yr, indicating that the PRB has experienced a decline in the maximum number of consecutive wet days in a year. The RX1day and CWD trends of Zhao et al. [65] were 0.11 mm/yr and −0.02 d/yr, respectively, which were slightly lower than our results.

3.1.2. Seasonal Trends

There was a seasonal trend observed in PRCPTOT, with an increase during summer and winter and a decrease during spring and autumn, indicating that there was an interannual and intraannual redistribution of precipitation. The highest average seasonal precipitation was observed in summer with 590.181 mm, while the lowest was obtained in winter with 106.721 mm. In addition, summer is the season with the highest absolute increasing rate (0.315 mm/yr) in precipitation. Spring decreased fastest, with a rate of 0.296 mm/yr. Zhang et al. [66] concluded that summer precipitation decreased in the PRB and winter precipitation increased, which is different from our results. The discrepancy is mostly due to the different time spans used. Zhang et al. only used data up to 2005, but our results used data up to 2015 (Figure 4(a1–a4)), causing different conclusions.

SDII showed an increasing trend in all seasons (Figure 4(b1–b4)), which was consistent with the conclusion of Liu et al. [22]. The highest average value is 9.80 mm/d in summer; the lowest average value is 5.23 mm/d in winter. The highest increasing rate is observed in winter, with a rate of 0.02 mm/d·yr; the lowest is observed in spring, with a rate of 0.002 mm/d·yr. In spring and autumn, the trend of SDII is opposite to that of PRCPTOT, illustrating that the precipitation has tended to be concentrated, and the possibility of drought and flood events in the basin has increased.

R95P also increased in four seasons (Figure 4(c1–c4)), the highest multi-year average is 136.326 mm obtained in summer and the lowest is 28.961 mm observed in winter. The highest increase rate was 0.135 mm/yr observed in winter; the lowest (0.046 mm/yr) was observed in spring. Zheng et al. [67] observed that the extreme precipitation in the PRB was increasing throughout the whole year, and the increasing is more noticeable in the dry season (winter, and a partial period of spring and autumn), which is consistent with our results.
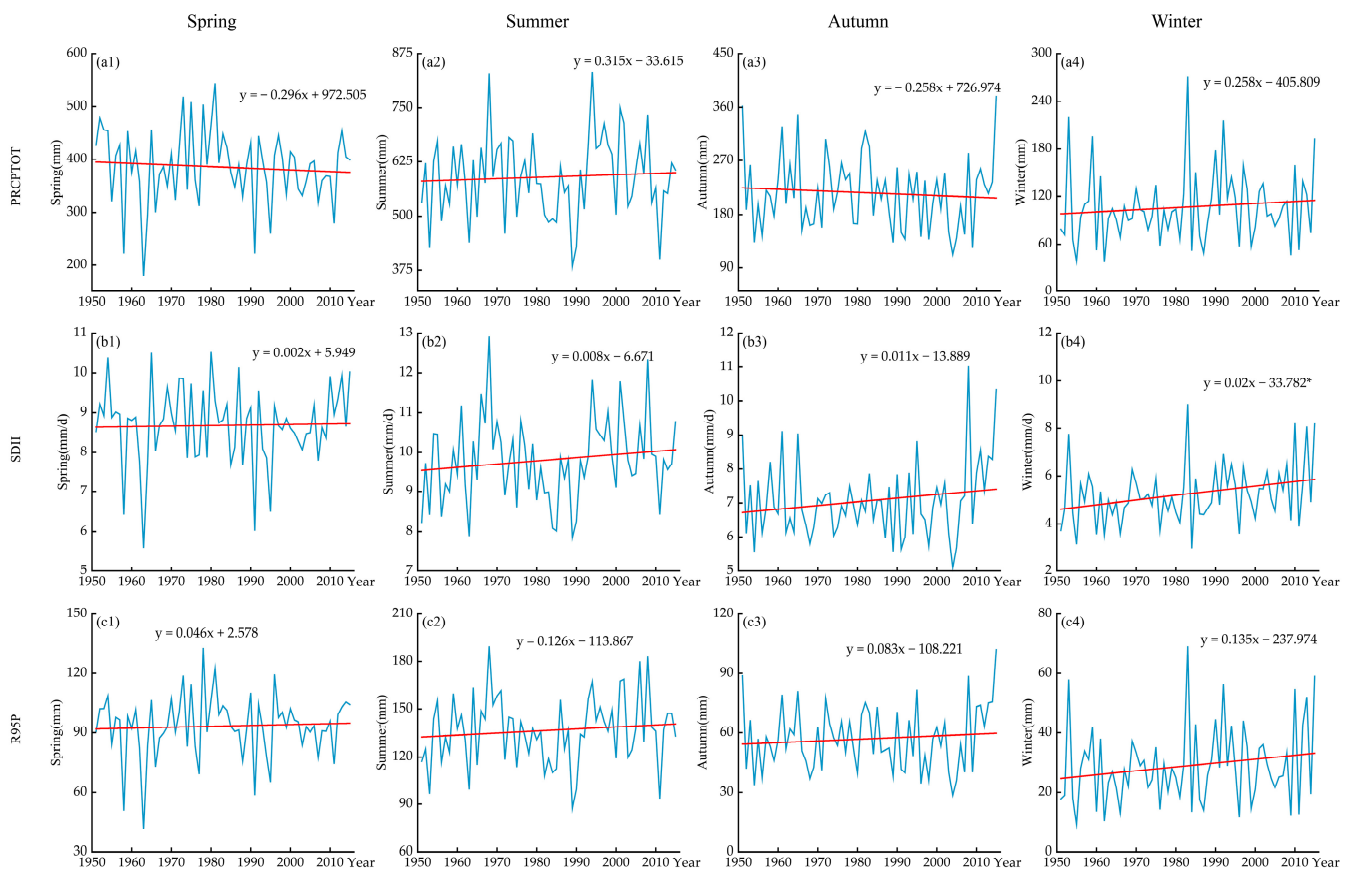
Figure 4. Temporal trends of EPIs in four seasons from 1951 to 2015; (**a1–a4**) PRCPTOT, (**b1–b4**) SDII, (**c1–c4**) R95P. * Significant at the level of 0.05.

3.2. Spatial Patterns

3.2.1. Annual Distributions

To better understand the spatial pattern of extreme precipitation in the PRB between 1951 and 2015, the distributions of annual and seasonal extreme precipitation indices were calculated at the pixel scale.

From the distribution of annual average PRCPTOT (Figure 5a), the total precipitation in the PRB is very high, but the regional distribution is uneven with gradient change from west to east, which was consistent with the results of Liu et al. [22]. The lowest PRCPTOT is 753.174 mm, which was located in the Yunnan–Guizhou Plateau of the upper reaches of the Xijiang River Basin (XRB); the highest PRCPTOT is 1905.810 mm, which was located at the border of the Dongjiang River Basin (DRB) and the Beijiang River Basin (BRB), mainly in the cities of Qingyuan and Guangzhou. The spatial pattern of annual average SDII resembles that of PRCPTOT (Figure 5b), and it was generally increasing from west to east. The highest value is 11.989 mm/d, which is concentrated in the DRB, and the lowest value is 5.549 mm/d, which is mainly in the Yunnan–Guizhou Plateau. The results suggest that the central and western PRB could experience a higher risk possibility of natural hazards, especially drought.

The annual distribution of R95P increases from west to east (Figure 5c) of the PRB. The highest annual average R95P is 476.151 mm, which was mainly distributed in the DRB; the lowest value is 151.879 mm, which was mainly in the upper reaches of the XRB. High values of R95P also appeared near the cities of Liuzhou and Guilin. The values of R95D range between 6.369 and 9.246 d, and most of the high values are concentrated in the middle and lower reaches of the XRB; they are mostly greater than 7 d, indicating that there is a greater frequency of extreme precipitation. Although the DRB has higher precipitation, R95D is still at a low level, and the number of days with extreme precipitation is relatively low.
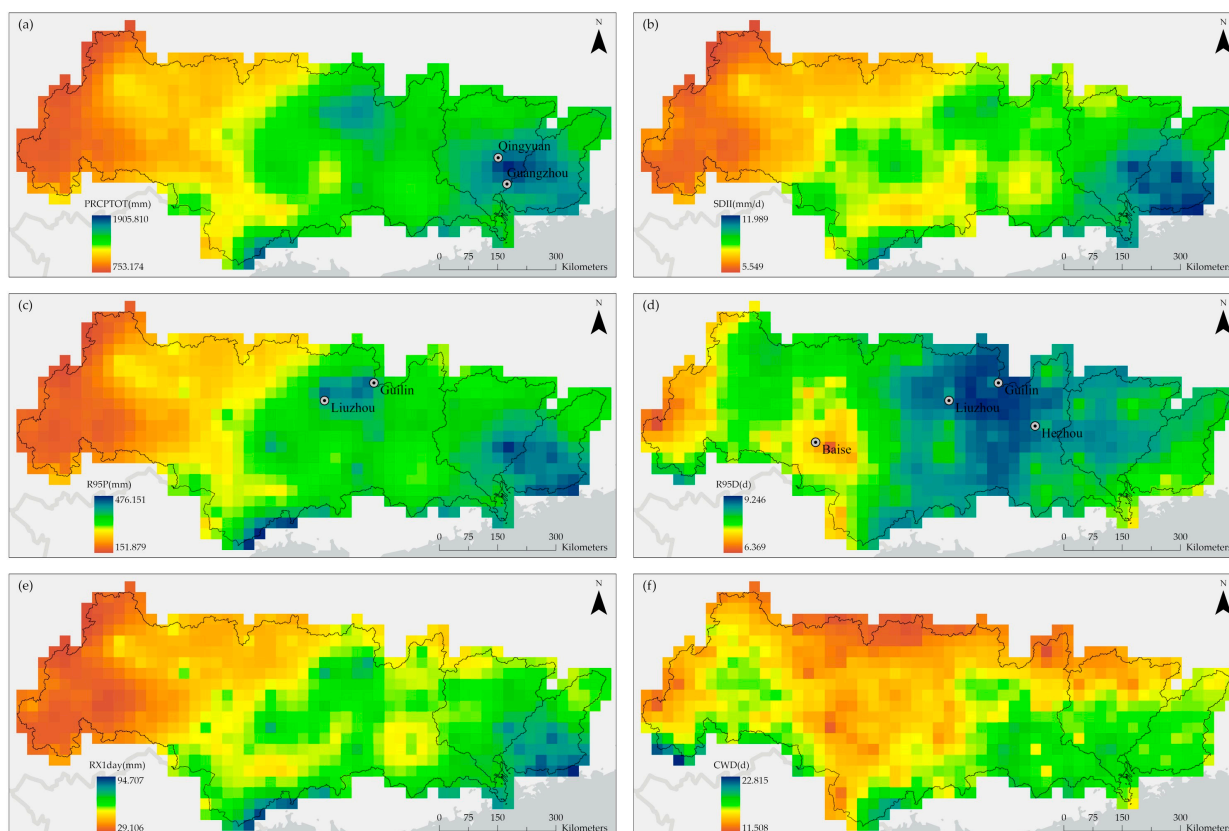
Figure 5. Spatial distributions of annual average EPIs in the PRB from 1951 to 2015; (**a**) PRCPTOT, (**b**) SDII, (**c**) R95P, (**d**) R95D, (**e**) RX1day, (**f**) CWD.

The multi-year trend of RX1day increases from west to east (Figure 5e), with the highest value of 94.707 mm, and the high values were mainly distributed in the DRB and BRB. The lowest value is 29.106 mm, and the low values are mainly distributed in the upper reaches of the XRB. The high value of RX1day is significantly greater than the threshold of extreme precipitation (50 mm/d) in China, which means that the possibility of extreme precipitation events and short-term floods in the BRB and DRB is higher than in other regions.

The annual distribution of CWD shows an increasing trend from northwest to south with a range between 11.508 and 22.815 d (Figure 5f). The major concentration of high values is in the downstream areas of the three major tributaries, and the low values are mainly located in the northeastern part of the PRB.

3.2.2. Seasonal Distributions

To explore the seasonal distribution patterns of precipitation, PRCPTOT, SDII, and R95P were selected for analysis.

According to the mean seasonal PRCPTOT (Figure 6(a1,b1,c1,d1)), summer and winter are the wettest and driest seasons, respectively. The spatial pattern in spring is comparable to annual distribution with the range from 110.201 to 719.195 mm. The main concentrations of high values are in the BRB and the DRB, corresponding to the low values distributed in the Yunnan–Guizhou Plateau. The summer precipitation increases from north to south fluctuating between 395.513 and 1002.331 mm. The highest values are mainly distributed near the cities of Dongguan and Huizhou. The lowest values are primarily distributed in the northern PRB. Precipitation in autumn has no significant spatial trend, ranging from 172.214 to 348.152 mm. The highest values are distributed in the southern PRB, and the lowest values are mainly distributed in the lower reaches of the XRB. The winter precipitation increases from west to east, ranging from 19.971 to 217.726 mm, with the

highest values near the cities of Guilin and Hezhou and the lowest values in the Yunnan–Guizhou Plateau. In addition, the winter precipitation near Zhongshan is much lower than the neighborhood areas. The overall spatial trend and absolute precipitation values of the four seasons are relatively close to the results from Deng et al. [38].
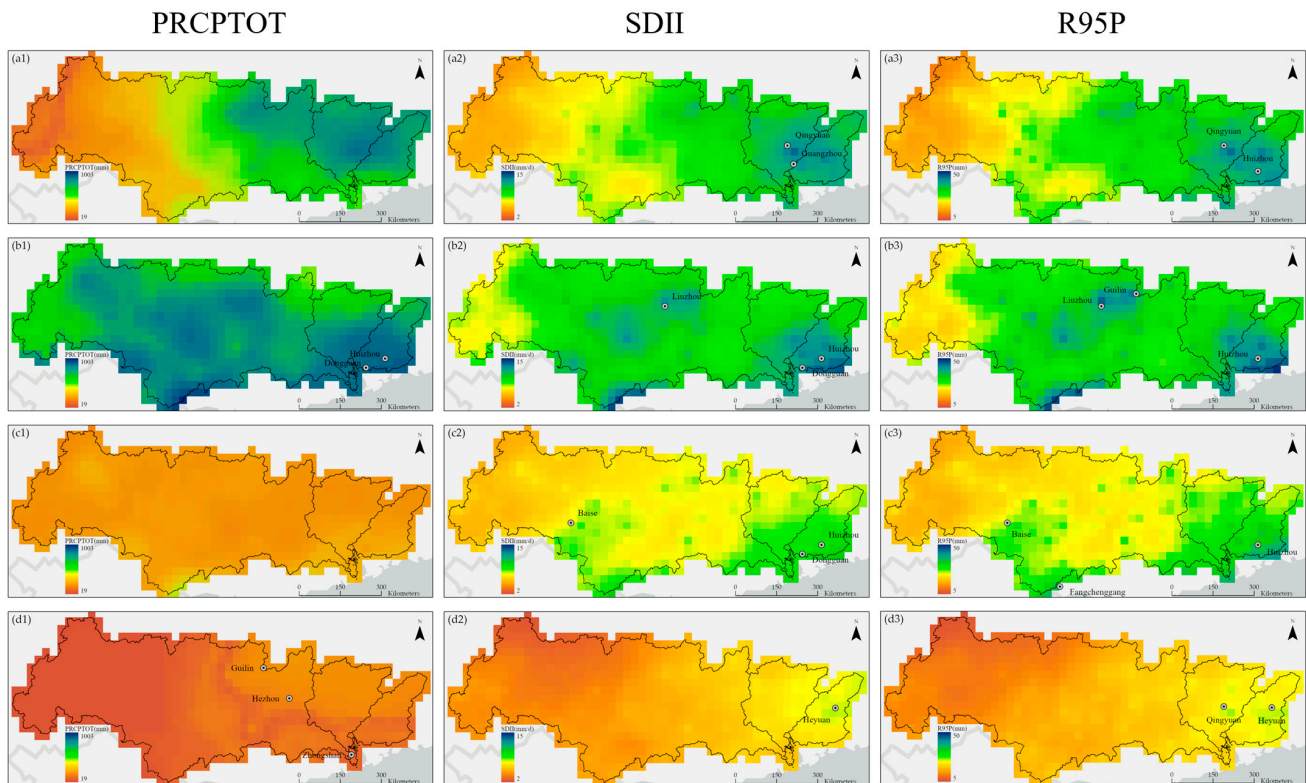
Figure 6. Spatial distributions of seasonal average EPIs in the PRB from 1951 to 2015; (**a1**–**a3**) Spring, (**b1**–**b3**) Summer, (**c1**–**c3**) Autumn, (**d1**–**d3**) Winter.

As shown in Figure 6(a2,b2,c2,d2), summer has the highest precipitation intensity while winter has the lowest in the PRB. The spatial distribution of spring SDII is similar to PRCPTOT, ranging from 4.251 to 13.595 mm/d and increasing from west to east. High values are mainly located near the cities of Qingyuan and Guangzhou, and the Yunnan–Guizhou Plateau is primarily characterized by low values. The precipitation intensity in summer has no significant trend, with the range between 6.906 and 14.481 mm/d. The SDII near Liuzhoul is higher than the neighborhood regions. The high values are mainly distributed near the cities of Dongguan and Huizhou, and the lowest values are distributed in the Yunnan–Guizhou Plateau. The gradient trend of SDII values in autumn and winter shows that the DRB has the highest values, while the upper reaches of the XRB have the lowest values. All in all, the BRB and the DRB obtained higher SDII and precipitation and thus have a relatively higher possibility of short-term floods.

According to the average seasonal R95P, the values in summer and winter are the highest and the lowest, respectively. The R95P in spring increases from west to east, ranging from 11.209 to 44.611 mm, with high values near the cities of Qingyuan and Huizhou and low values in the Yunnan–Guizhou Plateau. In summer, the average R95P tends to be lower in the west and higher in the east PRB, ranging from 18.814 to 49.561 mm. The high values are mainly near the cities of Huizhou, Liuzhou, and Guilin. In autumn, R95P values exhibit a northwest-to-southeast increase across the PRB, ranging from 13.735 to 40.366 mm. The highest values are near the city of Baise. The spatial distribution of R95P in winter was similar to autumn, but the high values in the DRB were more noticeable. The R95P results showed that the BRB and DRB displayed comparatively higher values for extreme precipitation among all the regions.

3.3. The M–K Test for the Spatiotemporal Trends

The M–K test was utilized to detect the spatiotemporal trend of extreme precipitation indices and the statistical significance of their change in the PRB.

As shown in Figure 7a, about 57.7% of the total area exhibited a decrease in PRCPTOT, with 3.2% decreased significantly, which was mainly observed in the upper reaches of the XRB. This region was located at higher elevations with relatively low precipitation, facing a high risk of droughts. Overall, 42.2% of the basin displayed an upward trend, primarily in the DRB and the BRB, but there was no area with a significant increase. Regarding SDII, 22.7% of the regions exhibited a decreasing tendency, which was mainly located in the upper reaches of the XRB. Overall, 77.3% of the regions showed an increasing trend, of which 37.3% showed a significant increase, which was mainly distributed in the DRB and BRB (Figure 7b). Zhang et al. [31] revealed that reduced annual precipitation was primarily observed in the western and south–central portions of the PRB, whereas significant decreases were concentrated in the northwestern regions of the basin, and about 74% of the stations have increased annual precipitation intensity, which was mainly located in the middle PRB and the PRD. Zhang et al.'s results are consistent with ours. An increase in precipitation intensity and slight increase in precipitation indicated that precipitation is more concentrated, which is a large challenge for flood control and mitigation in the PRD [68]. While in the XRB, especially in the upper reaches, the likelihood of drought is greater due to the decrease in both precipitation volume and intensity.
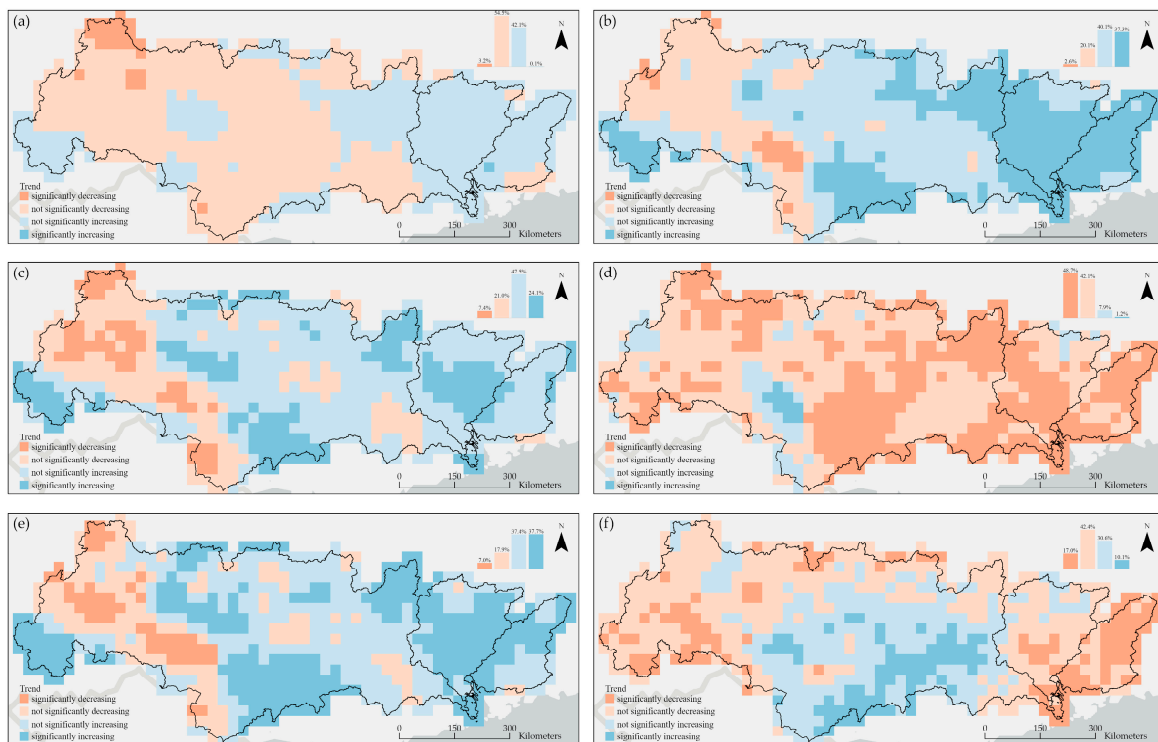
Figure 7. M–K test of EPIs; (**a**) PRCPTOT, (**b**) SDII, (**c**) R95P, (**d**) R95D, (**e**) RX1day, (**f**) CWD.

The tendency of R95P is similar to SDII (Figure 7c), 71.6% of the area showed an increasing trend. The regions that exhibited notable trends were primarily located in the BRB, as well as the middle reaches of the XRB, while the decreasing trend was predominantly observed in the upper reaches of the XRB, with 7.4% of the areas showing a significant decrease. However, almost the entire PRB (90.8%) showed a decreasing trend in R95D (Figure 7d). Therefore, it can be seen that there is a decreasing trend in R95P and R95D in the upper reaches of the XRB, indicating the possibility of short-term rainstorms and floods has decreased; but in other regions, although R95D decreased, the extreme precipitation increased, indicating that the intensity of extreme precipitation has been enhanced.

Approximately 75.1% of the total area displayed an increasing trend in RX1day (Figure 7e). The significant increases are mainly in the BRB and the lower reaches of XRB, indicating that more extreme precipitation events occurred in these regions, making runoff in these regions more concentrated [68] and easier to cause floods, while the significant reductions are obtained in the upper reaches of the XRB.

The DRB and BRB exhibited a decreasing trend in CWD (Figure 7f), while in the lower reaches of the XRB, mainly an increasing trend was derived, indicating that the trend of CWD in the PRB was not noticeable and remained at a relatively stable level. Overall, the fluctuations observed in these indices indicated a rise in the occurrence of extreme weather events, including but not limited to intense floods, droughts, and rainstorms in the PRB [69].

4. Discussion

4.1. Uncertainty Analysis

Previous studies have presented divergent findings on precipitation changes in the PRB. At the temporal scale, trends of annual precipitation exhibited a weak increase [70], insignificant changes [22,27,68,69], and insignificant decreases [65]. At the spatial scale, Deng et al. [71] showed that the eastern PRB had higher annual average precipitation but fewer rainy days from 1961 to 2008, but the western PRB had lower precipitation but more rainy days. Zhang et al. [31] indicated that the reduction in precipitation is concentrated predominantly in the middle and upper reaches of the PRB and the precipitation days decreased across the entire basin during 1960–2005, while the southeastern PRB experienced more precipitation [72]. For extreme precipitation, Peng et al. [68] reported that there are relatively large amounts of extreme precipitation in the central and eastern PRB from 1960 to 2005. Zhang et al. [31] observed a short-term increase in extreme precipitation, especially in the lower reaches of the Pearl River, and a significant increasing trend in both extreme precipitation amount and frequency during 1960–2005 [27]. Zhao et al. [65] found that the number of continuous wet days and heavy precipitation days shows an insignificant decrease during 1960–2012. Different time spans, the spatial resolution of precipitation data, and precipitation indices may lead to discrepancies in the results and conclusions. Our study has a longer time series and higher spatial resolution, probably providing a better representation of interannual and seasonal precipitation patterns and variability.

Although APHRODITE has been widely used for precipitation research and is considered as one of the most reliable precipitation datasets in Asia [73], related studies have demonstrated that it may underestimate precipitation compared to observations from meteorological stations [44,74,75]. To validate our results, this study compared the results from APHRODITE with China Meteorological Administration (CMA) data at temporal and spatial scales.

From 1951 to 2015, the annual average precipitation in the PRB obtained from the CMA was 1449.541 mm, while the corresponding results from the APHRODITE dataset was 1333.144 mm, which was slightly lower than the real observations. The overall temporal trend of APHRODITE was consistent with that from CMA data, but the results were slightly lower than those from CMA data (Figure 8). The correlation coefficient r is calculated to be 0.97, indicating an excellent temporal correlation.

On the basis of the spatial comparison (Figure 9), CMA data showed an increasing trend in annual precipitation from west to east in PRB, with values ranging from 797 to 2120 mm and the lowest values occurring in the upper reaches of the West River, while the highest values were mainly located in the Beijiang River Basin. The spatial distribution of APHRODITE data showed good agreement with that of CMA, but the values ranged from 753 to 1906 mm, which was slightly lower than those from CMA. Based on the above results, although the APHRODITE data were slightly lower than those from CMA, their spatiotemporal trends were similar, which have no substantial influence on the analysis of precipitation patterns in the PRB.
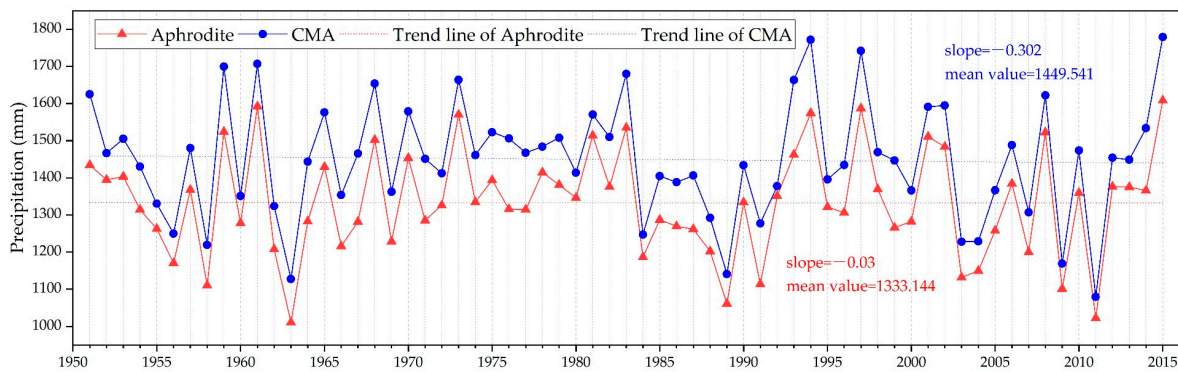
Figure 8. Comparisons of temporal changes and trend between APHRODITE and CMA data.

To check the accuracy of APHRODITE datasets, we employed MSWEP and CHIRPS precipitation datasets to make a comparison with CMA data at a monthly scale. As seen in Figure 10, these three datasets all have a strong relationship with the true precipitation. APHRODITE has the highest correlation coefficient with observations at meteorological stations ($R^2 = 0.99$). Although APHRODITE's spatial resolution is $0.25° \times 0.25°$, its accuracy is better than MSWEP ($0.1° \times 0.1°$) and CHIRPS ($0.05° \times 0.05°$). From Figure 10, it is evident that all three datasets yield accurate predictions for high precipitation events. However, their accuracy for low precipitation varies significantly, with the CHIRPS dataset performing the worst, which was followed by the MSWEP dataset. The CHIRPS dataset tends to overpredict low precipitation events, while the MSWEP dataset also exhibits some degree of overestimation, albeit it is less pronounced than the CHIRPS dataset (Figure 10). Furthermore, Figure 10 reveals that the statistical distributions of the MSWEP and CHIRPS datasets are relatively discrete, indicating substantial fluctuations in prediction accuracy across most stations, although the deviations appear to be randomly distributed. On the other hand, the results from the APHRODITE dataset demonstrate a more clustered pattern with lower uncertainty in the predictions. Through this comparison, it becomes apparent that while the MSWEP and CHIRPS datasets offer precipitation predictions with high accuracy and spatial resolution in regions such as Europe and North America, their prediction accuracy in Chinese regions is unsatisfactory. This discrepancy can be attributed to the limited number of meteorological stations in China from which the MSWEP and CHIRPS datasets are derived. In contrast, the APHRODITE dataset utilizes a more extensive set of observations from meteorological stations in China, resulting in improved simulation results. This is a crucial reason why we opted to use the APHRODITE dataset in our study.
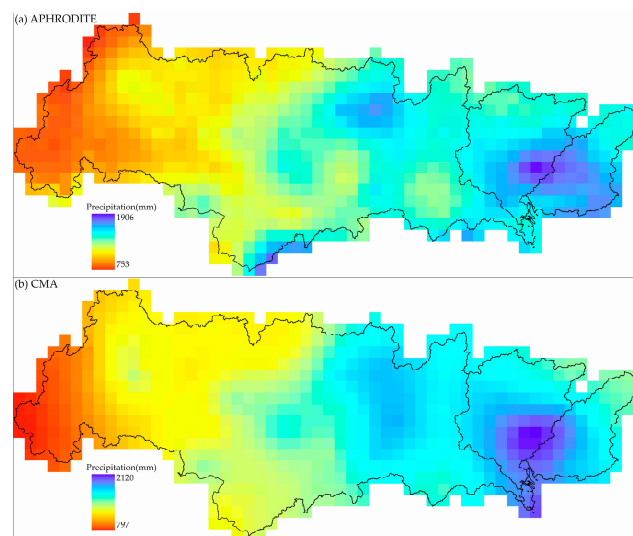

Figure 9. Comparison of spatial trend of annual mean precipitation between APHRODITE and CMA data from 1951 to 2015.
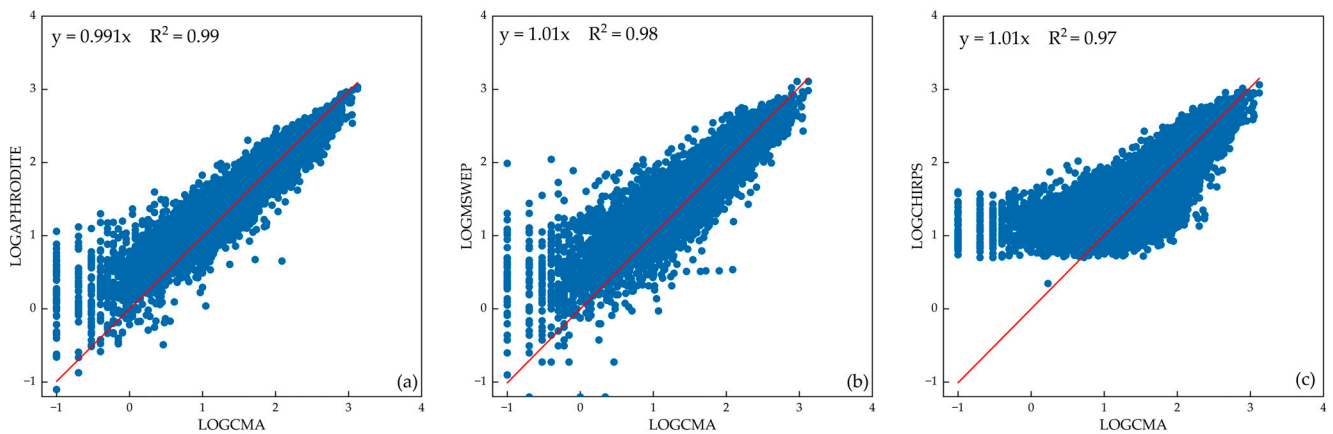
Figure 10. Comparison of monthly precipitation between different datasets and CMA data with log transformation from 1981 to 2015; (**a**) APHRODITE, (**b**) MSWEP, (**c**) CHIRPS.

### 4.2. Precipitation Changes between 2016 and 2022

Since APHRODITE's data are only available for the years before 2015, we also tested CHIRPS data to study the precipitation distribution from 2016 to 2022. Meanwhile, we also obtained rainfall observations from 2016 to 2021 from the Pearl River Water Conservancy Commission (PRWCC). Regarding the interannual variation (Figure 11a), it can be seen that in all years, CHIRPS data indicate an obvious overestimation due to the overestimation of low values discussed in the previous section. This also proves again that CHIRPS data have relatively high uncertainty in the PRB in China.
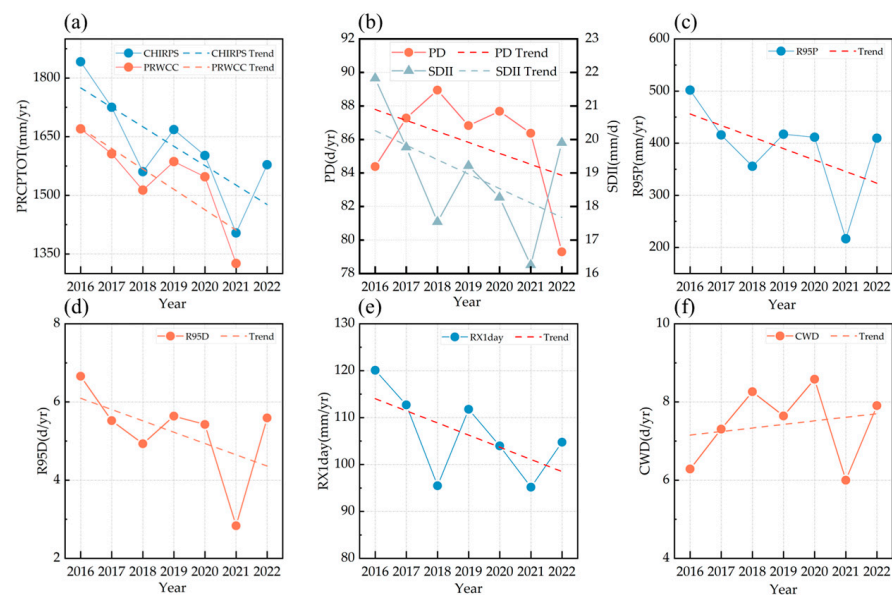

Figure 11. Temporal trends of EPIs from CHIRPS data between 2016 and 2022; (**a**) PRCPTOT, (**b**) PD & SDII, (**c**) R95P, (**d**) R95D, (**e**) RX1day, (**f**) CWD.

At the annual scale, except for CWD, all other EPIs show a decreasing trend, which indicated that the PRB was becoming slightly drier in these years (Figure 11). At the seasonal scale, there was a decreasing trend in PRCPTOT, SDII and R95P (Figure 12).

The spatial distribution of the annual average EPIs from 2016 to 2022 was similar with that between 1951 and 2015. The annual average SDII in Liuzhou city was higher than other regions in recent years (Figure 13), and the high values of RX1day were mainly located in the BRB. For the seasonal distributions, PRCPTOT and SDII have no significant trend in recent years, and R95P changes in spring and autumn (Figure 14).
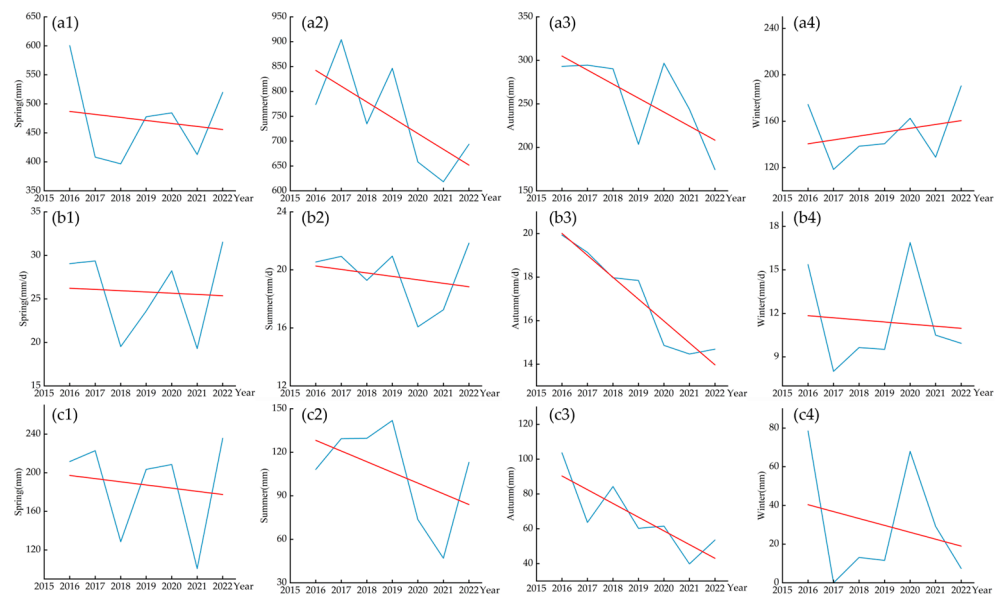
Figure 12. Temporal trends of EPIs in four seasons from CHIRPS data between 2016 and 2022; (**a1–a4**) PRCPTOT, (**b1–b4**) SDII, (**c1–c4**) R95P. Blue lines represent for values and red lines are the trends.
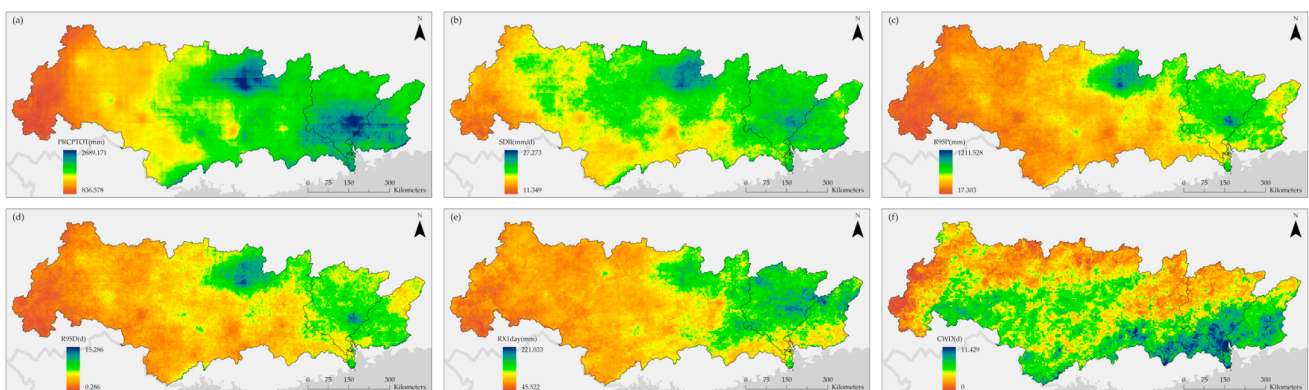
Figure 13. Spatial distributions of annual average EPIs in the PRB from CHIRPS data between 2016 and 2022; (**a**) PRCPTOT, (**b**) SDII, (**c**) R95P, (**d**) R95D, (**e**) RX1day, (**f**) CWD.

It is worth emphasizing that since CHIRPS data have a relatively high uncertainty in the PRB, and the analysis is based on only 7 years of data, the trend results may not be so reliable. To obtain a more accurate trend, more data with low uncertainty are necessary.

4.3. Possible Causes of Precipitation Changes

The mechanisms causing precipitation changes are extremely complex, which include the combined effects of the Asian monsoon, topography, and human activities.

Precipitation patterns in the PRB are primarily influenced by the Asian monsoon and moisture transport [76]. For example, one possible explanation for the decreasing trend in October precipitation could be attributed to the early onset of the East Asian winter monsoon, which is largely driven by shifts in wind direction [77]. The partition of dry and wet seasons is determined by the monthly moisture transport originating from the southwestern Pacific and Indian Ocean [29]. Additionally, more tropical cyclones will also lead to increased precipitation. The PRB is one of the regions affected by tropical cyclones. In the years with high precipitation, more tropical cyclones landed in the east of the basin, while in years with relatively low precipitation, fewer tropical cyclones landed, and these were seldomly into the remote areas in basin [71].
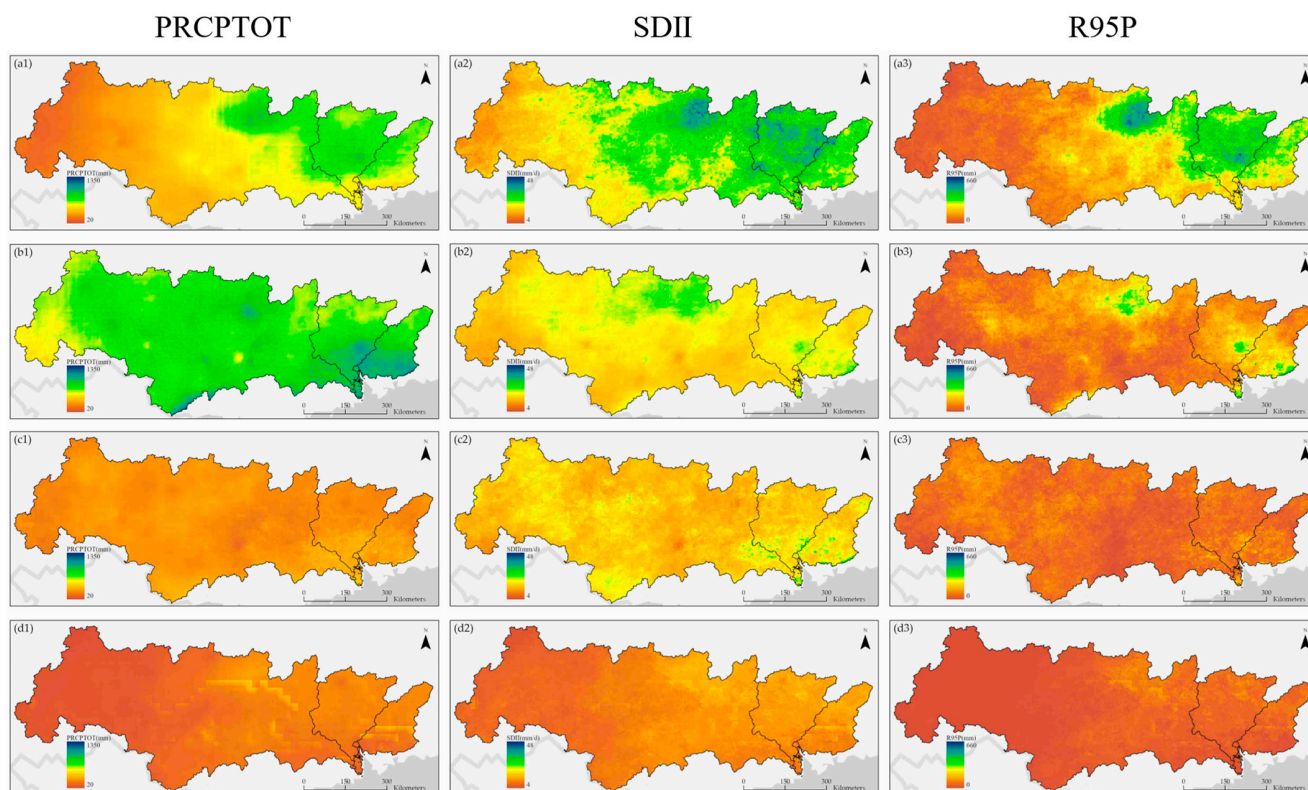
Figure 14. Spatial distributions of seasonal average EPIs in the PRB from CHIRPS data between 2016 and 2022; (**a1**–**a3**) Spring, (**b1**–**b3**) Summer, (**c1**–**c3**) Autumn, (**d1**–**d3**) Winter.

Topography (such as elevation, distance to the coast, and the influence of mountains) can also affect moisture input and derive different characteristics in different regions. In the northwest arid regions of China, the wetting trend increased with elevation [78], but the annual precipitation decreased with the increase in elevation from east to west in the Yangtze River Basin [79]. The complex and varied terrain in the Yellow River Basin also led to different climatic conditions and spatial variations of precipitation [80]. The PRB is characterized by a topography where higher terrain is found in the west and lower terrain is found in the east. The southeastern region is a relatively flat plain located on the windward side of mountains and hills, which is easier to be influenced by warm and moist air, subtropical high pressure, tropical cyclones, and typhoons, resulting in abundant precipitation [81]. The southwestern region is mountainous and relatively higher in altitude, and it obtains relatively low precipitation due to the weakened cold air input and the smaller influence of subtropical high pressure [82].

Human activities (such as greenhouse gas emissions, artificial heat, and fast urbanization) can also alter the local climate, thereby affecting precipitation patterns [83]. In densely populated urban areas, precipitation is more uncertain. An annual reduction in precipitation has been observed in the Beijing–Tianjin–Hebei urban agglomeration, whereas the Yangtze River Delta urban agglomeration has seen an increase in both annual and extreme precipitation [84]. In the PRB, precipitation events occur less frequently and for shorter durations in urban areas, such as the Pearl River Delta, compared to surrounding rural areas [85].

4.4. Correlation between Runoff and Precipitation

Liu et al. [86] showed that the interannual variation of the Pearl River runoff and precipitation have a great correlation between 1957 and 2009; Zhang et al. [87] also found that runoff changes in the PRB between 1948 and 2006 were mostly caused by precipitation changes. However, there are a few studies to reveal trends in recent decades. In this study, we conducted a simple validation of the APHRODITE data compared with the 2000–2015

runoff data from the PRWCC. As shown in Figure 15, the correlation coefficient in the entire PRB and its three sub-basins is satisfactory ($R^2 > 0.6$). Consistent with previous studies, precipitation has a huge impact on surface water resources in the PRB.
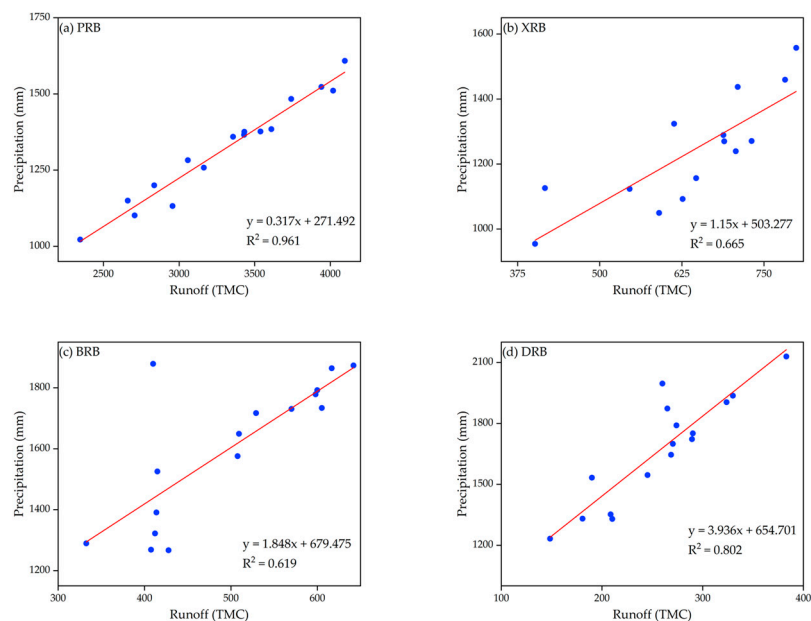
Figure 15. Correlation analysis between APHRODITE and runoff data; (**a**) PRB; (**b**) XRB; (**c**) BRB; (**d**) DRB.

4.5. The Impact of Precipitation Changes

Changes in extreme precipitation could directly cause floods in the PRB [72], and increased precipitation intensity and extreme precipitation frequency will enhance the risk of floods [3]. In addition, the dense river network of the PRB and the rugged terrain in the upper and middle reaches resulted in floods that occur with a rapid increase in water flow that reaches its peak when it merges into the mainstream [88], which makes flood prevention more difficult.

The PRB provides sufficient water resources, and it is accountable for the water supply of surrounding cities such as Macao and Hong Kong [89]. The basin's water supply is bound to suffer adverse effects as a result of increased annual precipitation intensity and extreme precipitation events coupled with a reduction in the number of rainy days [22]. Especially in the delta region, it is more difficult to supply fresh water because of the coastal location conditions.

Controlling soil erosion is of great importance for ecosystem management [35]. Over the past few years, the upper and middle reaches have undergone rapid economic growth, while human activities in the lower reaches have become progressively more intense, the water and soil conservation in the PRB has become increasingly difficult [90]. According to our results, extreme precipitation intensity increased in some regions, which may lead to intensified soil erosion. Relevant watershed management may face bigger challenges.

In general, understanding the temporal and spatial variation of precipitation in the PRB is of great significance for better water resources management, effective flood prevention, and sustainable basin development and environmental protection.

5. Conclusions

In this study, we used the APHRODITE dataset to calculate the seasonal and annual EPIs in the PRB and explore the temporal and spatial characteristics of precipitation changes. Based on the results, we obtained the following findings:

(1) At the temporal scale, the annual PRCPTOT showed a weak increasing trend. PD, R95D, and CWD decreased, but SDII, R95P, and RX1day showed an increasing trend,

leading to the increased short-term flood risk. The seasonal PRCPTOT showed an increase in summer and winter and a decrease in spring and autumn, while R95P and SDII showed an increasing trend in all seasons, and the precipitation tended to be concentrated in spring and autumn.

(2) At the spatial scale, the interannual variation of PRCPTOT increased from west to east. The distribution of SDII, R95P, and RX1day is spatially similar: the high value of R95D is located in the middle and lower reaches of the XRB, and the CWD increased from north to south. The spatial distributions of seasonal PRCPTOT, SDII, and R95P were also similar, showing an increase from west to east in spring and winter, and gradually increasing from north to south in summer, revealing that the BRB and the DRB have higher flood risks.

(3) The M–K test results showed that the upper reaches of the XRB have become drier, especially in the Yunnan–Guizhou Plateau. The PRD has a higher flood risk. The joint changes in EPIs have revealed the higher occurrence of extreme weather events in the PRB.

References

1. Allen, M.R.; Ingram, W.J. Constraints on future changes in climate and the hydrologic cycle. *Nature* **2002**, *419*, 224–232. [CrossRef] [PubMed]
2. AghaKouchak, A.; Sorooshian, S.; Arkin, P.; Eylander, J.; Foufoula-Georgiou, E.; Harmon, R.; Hendrickx, J.M.H.; Imam, B.; Kuligowski, R.; Skahill, B.; et al. Advanced Concepts on Remote Sensing of Precipitation at Multiple Scales. *Bull. Am. Meteorol. Soc.* **2011**, *92*, 1353–1357. [CrossRef]
3. Zhang, Q.; Xu, C.-Y.; Gemmer, M.; Chen, Y.D.; Liu, C. Changing properties of precipitation concentration in the Pearl River basin, China. *Stoch. Environ. Res. Risk Assess.* **2008**, *23*, 377–385. [CrossRef]
4. Zhang, M.; He, J.; Wang, B.; Wang, S.; Li, S.; Liu, W.; Ma, X. Extreme drought changes in Southwest China from 1960 to 2009. *J. Geogr. Sci.* **2013**, *23*, 3–16. [CrossRef]
5. Huang, J.; Liu, Y.; Ma, L.; Su, F. Methodology for the assessment and classification of regional vulnerability to natural hazards in China: The application of a DEA model. *Nat. Hazards* **2012**, *65*, 115–134. [CrossRef]
6. Su, Y.; Zhao, C.; Wang, Y.; Ma, Z. Spatiotemporal Variations of Precipitation in China Using Surface Gauge Observations from 1961 to 2016. *Atmosphere* **2020**, *11*, 303. [CrossRef]
7. Qian, W.-H.; Lin, X. Regional trends in recent precipitation indices in China. *Meteorol. Atmos. Phys.* **2005**, *90*, 193–207. [CrossRef]
8. Liu, B.; Xu, M.; Henderson, M.; Qi, Y. Observed trends of precipitation amount, frequency, and intensity in China, 1960–2000. *J. Geophys. Res. Atmos.* **2005**, *110*, D08103. [CrossRef]
9. Suhaila, J.; Deni, S.M.; Wan Zin, W.Z.; Jemain, A.A. Spatial patterns and trends of daily rainfall regime in Peninsular Malaysia during the southwest and northeast monsoons: 1975–2004. *Meteorol. Atmos. Phys.* **2010**, *110*, 1–18. [CrossRef]
10. Bhutiyani, M.R.; Kale, V.S.; Pawar, N.J. Climate change and the precipitation variations in the northwestern Himalaya: 1866–2006. *Int. J. Climatol.* **2010**, *30*, 535–548. [CrossRef]
11. Wang, B.; Ding, Q. Changes in global monsoon precipitation over the past 56 years. *Geophys. Res. Lett.* **2006**, *33*. [CrossRef]
12. Wendler, G.; Gordon, T.; Stuefer, M. On the Precipitation and Precipitation Change in Alaska. *Atmosphere* **2017**, *8*, 253. [CrossRef]

13. Zolina, O.; Simmer, C.; Gulev, S.K.; Kollet, S. Changing structure of European precipitation: Longer wet periods leading to more abundant rainfalls. *Geophys. Res. Lett.* **2010**, *37*. [CrossRef]

14. Che Mat Nor, S.M.; Shaharudin, S.M.; Ismail, S.; Mohd Najib, S.A.; Tan, M.L.; Ahmad, N. Statistical Modeling of RPCA-FCM in Spatiotemporal Rainfall Patterns Recognition. *Atmosphere* **2022**, *13*, 145. [CrossRef]

15. Zhai, P.; Zhang, X.; Wan, H.; Pan, X. Trends in total precipitation and frequency of daily precipitation extremes over China. *J. Clim.* **2005**, *18*, 1096–1108. [CrossRef]

16. Zhang, Q.; Sun, P.; Singh, V.P.; Chen, X. Spatial-temporal precipitation changes (1956–2000) and their implications for agriculture in China. *Glob. Planet. Change* **2012**, *82–83*, 86–95. [CrossRef]

17. Song, Y.; Achberger, C.; Linderholm, H.W. Rain-season trends in precipitation and their effect in different climate regions of China during 1961–2008. *Environ. Res. Lett.* **2011**, *6*, 034025. [CrossRef]

18. Zhang, X.; Cong, Z. Trends of precipitation intensity and frequency in hydrological regions of China from 1956 to 2005. *Glob. Planet. Chang.* **2014**, *117*, 40–51. [CrossRef]

19. Qu, B.; Lv, A.; Jia, S.; Zhu, W. Daily Precipitation Changes over Large River Basins in China, 1960–2013. *Water* **2016**, *8*, 185. [CrossRef]

20. Jiang, T.; Su, B.; Hartmann, H. Temporal and spatial trends of precipitation and river flow in the Yangtze River Basin, 1961–2000. *Geomorphology* **2007**, *85*, 143–154. [CrossRef]

21. Zhang, Q.; Peng, J.; Singh, V.P.; Li, J.; Chen, Y.D. Spatio-temporal variations of precipitation in arid and semiarid regions of China: The Yellow River basin as a case study. *Glob. Planet. Chang.* **2014**, *114*, 38–49. [CrossRef]

22. Liu, B.; Chen, J.; Lu, W.; Chen, X.; Lian, Y. Spatiotemporal characteristics of precipitation changes in the Pearl River Basin, China. *Theor. Appl. Climatol.* **2015**, *123*, 537–550. [CrossRef]

23. Duncan, J.M.A.; Biggs, E.M. Assessing the accuracy and applied use of satellite-derived precipitation estimates over Nepal. *Appl. Geogr.* **2012**, *34*, 626–638. [CrossRef]

24. Peña-Arancibia, J.L.; van Dijk, A.I.J.M.; Renzullo, L.J.; Mulligan, M. Evaluation of Precipitation Estimation Accuracy in Reanalyses, Satellite Products, and an Ensemble Method for Regions in Australia and South and East Asia. *J. Hydrometeor.* **2013**, *14*, 1323–1333. [CrossRef]

25. Khandu; Awange, J.L.; Kuhn, M.; Anyah, R.; Forootan, E. Changes and variability of precipitation and temperature in the Ganges-Brahmaputra-Meghna River Basin based on global high-resolution reanalyses. *Int. J. Climatol.* **2017**, *37*, 2141–2159. [CrossRef]

26. Yang, T.; Zhang, Q.; Chen, Y.D.; Tao, X.; Xu, C.-Y.; Chen, X. A spatial assessment of hydrologic alteration caused by dam construction in the middle and lower Yellow River, China. *Hydrol. Process.* **2008**, *22*, 3829–3843. [CrossRef]

27. Zhang, Q.; Xu, C.Y.; Becker, S.; Zhang, Z.X.; Chen, Y.D.; Coulibaly, M. Trends and abrupt changes of precipitation maxima in the Pearl River basin, China. *Atmos. Sci. Lett.* **2009**, *10*, 132–144. [CrossRef]

28. Cao, B.; Qiu, J.; Zhang, W.; Xie, X.; Lu, X.; Yang, X.; Li, H. Retrieval of Suspended Sediment Concentrations in the Pearl River Estuary Using Multi-Source Satellite Imagery. *Remote Sens.* **2022**, *14*, 3896. [CrossRef]

29. Yang, T.; Shao, Q.; Hao, Z.-C.; Chen, X.; Zhang, Z.; Xu, C.-Y.; Sun, L. Regional frequency analysis and spatio-temporal pattern characterization of rainfall extremes in the Pearl River Basin, China. *J. Hydrol.* **2010**, *380*, 386–405. [CrossRef]

30. Duan, L.; Zheng, J.; Li, W.; Liu, T.; Luo, Y. Multivariate properties of extreme precipitation events in the Pearl River basin, China: Magnitude, frequency, timing, and related causes. *Hydrol. Process.* **2017**, *31*, 3662–3671. [CrossRef]

31. Zhang, Q.; Singh, V.P.; Peng, J.; Chen, Y.D.; Li, J. Spatial–temporal changes of precipitation structure across the Pearl River basin, China. *J. Hydrol.* **2012**, *440–441*, 113–122. [CrossRef]

32. Zhang, W.; Cheng, Z.; Qiu, J.; Park, E.; Ran, L.; Xie, X.; Yang, X. Spatiotemporal Changes in Mulberry-Dyke-Fish Ponds in the Guangdong-Hong Kong-Macao Greater Bay Area over the Past 40 Years. *Water* **2021**, *13*, 2953. [CrossRef]

33. Wong, J.S.; Zhang, Q.; Chen, Y.D. Statistical modeling of daily urban water consumption in Hong Kong: Trend, changing patterns, and forecast. *Water Resour. Res.* **2010**, *46*. [CrossRef]

34. Niu, K.; Qiu, J.; Cai, S.; Zhang, W.; Mu, X.; Park, E.; Yang, X. Use of a MODIS Satellite-Based Aridity Index to Monitor Drought Conditions in the Pearl River Basin from 2001 to 2021. *ISPRS Int. J. Geo-Inf.* **2022**, *11*, 541. [CrossRef]

35. Mu, X.; Qiu, J.; Cao, B.; Cai, S.; Niu, K.; Yang, X. Mapping Soil Erosion Dynamics (1990–2020) in the Pearl River Basin. *Remote Sens.* **2022**, *14*, 5949. [CrossRef]

36. Liu, Y.; Chen, C. Pearl River Basin Flood Season Rainfall Evolution Characteristics. *Pearl River* **2007**, *28*, 47–51. [CrossRef]

37. Qiu, J.; Cao, B.; Park, E.; Yang, X.; Zhang, W.; Tarolli, P. Flood Monitoring in Rural Areas of the Pearl River Basin (China) Using Sentinel-1 SAR. *Remote Sens.* **2021**, *13*, 1384. [CrossRef]

38. Deng, S.; Chen, T.; Yang, N.; Qu, L.; Li, M.; Chen, D. Spatial and temporal distribution of rainfall and drought characteristics across the Pearl River basin. *Sci. Total Environ.* **2018**, *619–620*, 28–41. [CrossRef]

39. Onogi, K.; Koide, H.; Sakamoto, M.; Kobayashi, S.; Tsutsui, J.; Hatsushika, H.; Matsumoto, T.; Yamazaki, N.; Kamahori, H.; Takahashi, K.; et al. JRA-25: Japanese 25-year re-analysis project—Progress and status. *Q. J. R. Meteorol. Soc.* **2005**, *131*, 3259–3268. [CrossRef]

40. Uppala, S.M.; KÅllberg, P.W.; Simmons, A.J.; Andrae, U.; Bechtold, V.D.C.; Fiorino, M.; Gibson, J.K.; Haseler, J.; Hernandez, A.; Kelly, G.A.; et al. The ERA-40 re-analysis. *Q. J. R. Meteorol. Soc.* **2005**, *131*, 2961–3012. [CrossRef]

41. Saha, S.; Moorthi, S.; Pan, H.-L.; Wu, X.; Wang, J.; Nadiga, S.; Tripp, P.; Kistler, R.; Woollen, J.; Behringer, D.; et al. The NCEP Climate Forecast System Reanalysis. *Bull. Am. Meteorol. Soc.* **2010**, *91*, 1015–1058. [CrossRef]
42. Woollen, J.; Sienkiewicz, M.; Ruddick, A.G.; Robertson, F.R.; Reichle, R.; Redder, C.R.; Pegion, P.; Pawson, S.; Owens, T.; Molod, A.; et al. MERRA: NASA's Modern-Era Retrospective Analysis for Research and Applications. *J. Clim.* **2011**, *24*, 3624–3648. [CrossRef]
43. Andermann, C.; Bonnet, S.; Gloaguen, R. Evaluation of precipitation data sets along the Himalayan front. *Geochem. Geophys. Geosyst.* **2011**, *12*, Q07023. [CrossRef]
44. Tong, K.; Su, F.; Yang, D.; Zhang, L.; Hao, Z. Tibetan Plateau precipitation as depicted by gauge observations, reanalyses and satellite retrievals. *Int. J. Climatol.* **2014**, *34*, 265–285. [CrossRef]
45. Prakash, S.; Mitra, A.K.; Momin, I.M.; Rajagopal, E.N.; Basu, S.; Collins, M.; Turner, A.G.; Achuta Rao, K.; Ashok, K. Seasonal intercomparison of observational rainfall datasets over India during the southwest monsoon season. *Int. J. Climatol.* **2015**, *35*, 2326–2338. [CrossRef]
46. Kishore, P.; Jyothi, S.; Basha, G.; Rao, S.V.B.; Rajeevan, M.; Velicogna, I.; Sutterley, T.C. Precipitation climatology over India: Validation with observations and reanalysis datasets and spatial trends. *Clim. Dyn.* **2015**, *46*, 541–556. [CrossRef]
47. Renwick, J.; McGregor, J.; Rana, S. Precipitation Seasonality over the Indian Subcontinent: An Evaluation of Gauge, Reanalyses, and Satellite Retrievals. *J. Hydrometeorol.* **2015**, *16*, 631–651. [CrossRef]
48. Hamada, A.; Arakawa, O.; Yatagai, A. An automated quality control method for daily rain-gauge data. *Global Environ. Res.* **2011**, *15*, 183–192.
49. Yatagai, A.; Arakawa, O.; Kamiguchi, K.; Kawamoto, H.; Nodzu, M.I.; Hamada, A. A 44-Year Daily Gridded Precipitation Dataset for Asia Based on a Dense Network of Rain Gauges. *Sola* **2009**, *5*, 137–140. [CrossRef]
50. Yatagai, A.; Kamiguchi, K.; Arakawa, O.; Hamada, A.; Yasutomi, N.; Kitoh, A. APHRODITE: Constructing a Long-Term Daily Gridded Precipitation Dataset for Asia Based on a Dense Network of Rain Gauges. *Bull. Am. Meteorol. Soc.* **2012**, *93*, 1401–1415. [CrossRef]
51. Feng, S.; Hu, Q.; Qian, W. Quality control of daily meteorological data in China, 1951–2000: A new dataset. *Int. J. Climatol.* **2004**, *24*, 853–870. [CrossRef]
52. Beck, H.E.; Wood, E.F.; Pan, M.; Fisher, C.K.; Miralles, D.G.; van Dijk, A.I.J.M.; McVicar, T.R.; Adler, R.F. MSWEP V2 Global 3-Hourly 0.1° Precipitation: Methodology and Quantitative Assessment. *Bull. Am. Meteorol. Soc.* **2019**, *100*, 473–500. [CrossRef]
53. Funk, C.; Peterson, P.; Landsfeld, M.; Pedreros, D.; Verdin, J.; Shukla, S.; Husak, G.; Rowland, J.; Harrison, L.; Hoell, A.; et al. The climate hazards infrared precipitation with stations—A new environmental record for monitoring extremes. *Sci. Data* **2015**, *2*, 150066. [CrossRef] [PubMed]
54. Costa, A.C.; Soares, A. Trends in extreme precipitation indices derived from a daily rainfall database for the South of Portugal. *Int. J. Climatol.* **2009**, *29*, 1956–1975. [CrossRef]
55. Tramblay, Y.; El Adlouni, S.; Servat, E. Trends and variability in extreme precipitation indices over Maghreb countries. *Nat. Hazards Earth Syst. Sci.* **2013**, *13*, 3235–3248. [CrossRef]
56. de Lima, M.I.P.; Santo, F.E.; Ramos, A.M.; Trigo, R.M. Trends and correlations in annual extreme precipitation indices for mainland Portugal, 1941–2007. *Theor. Appl. Climatol.* **2014**, *119*, 55–75. [CrossRef]
57. Bhatti, A.S.; Wang, G.; Ullah, W.; Ullah, S.; Fiifi Tawia Hagan, D.; Kwesi Nooni, I.; Lou, D.; Ullah, I. Trend in Extreme Precipitation Indices Based on Long Term In Situ Precipitation Records over Pakistan. *Water* **2020**, *12*, 797. [CrossRef]
58. Ryan, C.; Curley, M.; Walsh, S.; Murphy, C. Long-term trends in extreme precipitation indices in Ireland. *Int. J. Climatol.* **2021**, *42*, 4040–4061. [CrossRef]
59. Mann, H.B. Nonparametric tests against trend. *Econ. J. Econ. Soc.* **1945**, *13*, 245–259. [CrossRef]
60. Xu, K.; Milliman, J.D.; Xu, H. Temporal trend of precipitation and runoff in major Chinese Rivers since 1951. *Glob. Planet. Chang.* **2010**, *73*, 219–232. [CrossRef]
61. Fu, G.; Yu, J.; Yu, X.; Ouyang, R.; Zhang, Y.; Wang, P.; Liu, W.; Min, L. Temporal variation of extreme rainfall events in China, 1961–2009. *J. Hydrol.* **2013**, *487*, 48–59. [CrossRef]
62. Łupikasza, E.B.; Hänsel, S.; Matschullat, J. Regional and seasonal variability of extreme precipitation trends in southern Poland and central-eastern Germany 1951–2006. *Int. J. Climatol.* **2011**, *31*, 2249–2271. [CrossRef]
63. Sen, P.K. Estimates of the Regression Coefficient Based on Kendall's Tau. *J. Am. Stat. Assoc.* **1968**, *63*, 1379–1389. [CrossRef]
64. Partal, T.; Kahya, E. Trend analysis in Turkish precipitation data. *Hydrol. Process.* **2006**, *20*, 2011–2026. [CrossRef]
65. Zhao, Y.; Zou, X.; Cao, L.; Xu, X. Changes in precipitation extremes over the Pearl River Basin, southern China, during 1960–2012. *Quat. Int.* **2014**, *333*, 26–39. [CrossRef]
66. Zhang, Q.; Xu, C.Y.; Zhang, Z.; Chen, Y.D.; Liu, C.L. Spatial and temporal variability of precipitation over China, 1951–2005. *Theor. Appl. Climatol.* **2008**, *95*, 53–68. [CrossRef]
67. Zheng, J.; Zhang, Q.; Shi, P.; Gu, X.; Zheng, Y. Spatiotemporal Characteristics of Extreme Precipitation Regimes and Related Driving Factors in the Pearl River Basin. *Sci. Geogr. Sin.* **2017**, *37*, 283–291.
68. Peng, J.; Zhang, Q.; Liu, C. Changing properties of precipitation regimes over the Pearl River Basin. *Pearl River* **2012**, *33*, 13–17.
69. Fischer, T.; Gemmer, M.; Lüliu, L.; Buda, S. Temperature and precipitation trends and dryness/wetness pattern in the Zhujiang River Basin, South China, 1961–2007. *Quat. Int.* **2011**, *244*, 138–148. [CrossRef]

70. Lu, W.; Liu, B.; Chen, J.; Chen, X. Variation Trend of Precipitation in the Pearl River Basin in Recent 50 Years. *J. Nat. Resour.* **2014**, *29*, 80–90. [CrossRef]

71. Deng, H.; Luo, Y. Analysis of spatial and temporal distributions of rainfall in Zhujiang river basin in the past 50 a. *J. Meteorol. Sci.* **2013**, *33*, 355–361.

72. Zhang, Q.; Xu, C.-Y.; Zhang, Z. Observed changes of drought/wetness episodes in the Pearl River basin, China, using the standardized precipitation index and aridity index. *Theor. Appl. Climatol.* **2009**, *98*, 89–99. [CrossRef]

73. Ménégoz, M.; Gallée, H.; Jacobi, H.W. Precipitation and snow cover in the Himalaya: From reanalysis to regional climate simulations. *Hydrol. Earth Syst. Sci.* **2013**, *17*, 3921–3936. [CrossRef]

74. Ono, K.; Kazama, S. Analysis of extreme daily rainfall in Southeast Asia with a gridded daily rainfall data set. *IAHS Publ.* **2011**, *344*, 169–175.

75. Immerzeel, W.W.; Wanders, N.; Lutz, A.F.; Shea, J.M.; Bierkens, M.F.P. Reconciling high-altitude precipitation in the upper Indus basin with glacier mass balances and runoff. *Hydrol. Earth Syst. Sci.* **2015**, *19*, 4673–4687. [CrossRef]

76. Yu, Z.-G.; Leung, Y.; Chen, Y.D.; Zhang, Q.; Anh, V.; Zhou, Y. Multifractal analyses of daily rainfall time series in Pearl River basin of China. *Phys. A Stat. Mech. Its Appl.* **2014**, *405*, 193–202. [CrossRef]

77. Fischer, T.; Gemmer, M.; Jiang, T.; Su, B.; Liu, L.L. Trends in Precipitation Extremes in the Zhujiang River Basin, South China. *J. Clim.* **2011**, *24*, 750–761. [CrossRef]

78. Yao, J.; Yang, Q.; Mao, W.; Zhao, Y.; Xu, X. Precipitation trend–Elevation relationship in arid regions of the China. *Glob. Planet. Chang.* **2016**, *143*, 1–9. [CrossRef]

79. Li, X.; Zhang, K.; Gu, P.; Feng, H.; Yin, Y.; Chen, W.; Cheng, B. Changes in precipitation extremes in the Yangtze River Basin during 1960–2019 and the association with global warming, ENSO, and local effects. *Sci. Total Environ.* **2021**, *760*, 144244. [CrossRef]

80. Liu, Q.; Yang, Z.; Cui, B. Spatial and temporal variability of annual precipitation during 1961–2006 in Yellow River Basin, China. *J. Hydrol.* **2008**, *361*, 330–338. [CrossRef]

81. Lu, W.; Liu, B.; Chen, X.; Wu, L. Characteristics of Precipitation Period in Pearl River Basin. *J. China Hydrol.* **2013**, *33*, 82–86.

82. Tang, Y.; Chen, X. Multi-scale Spatio-temporal Characteristics and Influence of Precipitation Variation in Zhujiang River Basin During the Last 50 Years. *Sci. Geogtaphica Sin.* **2015**, *35*, 476–482.

83. Han, J.-Y.; Baik, J.-J.; Lee, H. Urban impacts on precipitation. *Asia-Pac. J. Atmos. Sci.* **2014**, *50*, 17–30. [CrossRef]

84. Li, W.; He, X.; Scaioni, M.; Yao, D.; Mi, C.; Zhao, J.; Chen, Y.; Zhang, K.; Gao, J.; Li, X. Annual precipitation and daily extreme precipitation distribution: Possible trends from 1960 to 2010 in urban areas of China. *Geomat. Nat. Hazards Risk* **2019**, *10*, 1694–1711. [CrossRef]

85. Chen, S.; Li, W.-B.; Du, Y.-D.; Mao, C.-Y.; Zhang, L. Urbanization effect on precipitation over the Pearl River Delta based on CMORPH data. *Adv. Clim. Chang. Res.* **2015**, *6*, 16–22. [CrossRef]

86. Liu, F.; Yuan, L.; Yang, Q.; Ou, S.; Xie, L.; Cui, X. Hydrological responses to the combined influence of diverse human activities in the Pearl River delta, China. *Catena* **2014**, *113*, 41–55. [CrossRef]

87. Zhang, Q.; Xu, C.-Y.; Zhang, Z.; Chen, Y.D. Changes of atmospheric water vapor budget in the Pearl River basin and possible implications for hydrological cycle. *Theor. Appl. Climatol.* **2010**, *102*, 185–195. [CrossRef]

88. Wu, Z.-Y.; Lu, G.-H.; Liu, Z.-Y.; Wang, J.-X.; Xiao, H. Trends of Extreme Flood Events in the Pearl River Basin during 1951–2010. *Adv. Clim. Chang. Res.* **2013**, *4*, 110–116. [CrossRef]

89. Chen, Y.D.; Zhang, Q.; Chen, X.; Wang, P. Multiscale variability of streamflow changes in the Pearl River basin, China. *Stoch. Environ. Res. Risk Assess.* **2011**, *26*, 235–246. [CrossRef]

90. Lai, C.; Chen, X.; Wang, Z.; Wu, X.; Zhao, S.; Wu, X.; Bai, W. Spatio-temporal variation in rainfall erosivity during 1960–2012 in the Pearl River Basin, China. *Catena* **2016**, *137*, 382–391. [CrossRef]